Simulations of Meniscus Motion and Evaporation for Convective Deposition Manufacturing

Junfeng Xiao[1*] and Daniel Attinger[1]
[1]Department of Mechanical Engineering, Columbia University
*Corresponding author: 249 S.W. Mudd Building, 500 West 120th Street, New York, NY 10027, email: jx2151@columbia.edu

Abstract: Convective deposition is a convenient and rapid manufacturing process used to deposit uniform micro- and nano-particle crystal. Convective deposition is a typical multiphysics transport process driven by evaporation of a moving meniscus. In this work we solve fluid dynamics, heat transfer and mass transfer equations in a deforming geometry using a moving mesh (Arbitrary Lagrangian-Euler, ALE) method. Weak form equations for mesh deformation, fluid dynamics, heat transfer and mass transfer are derived in order to be implemented in COMSOL, and a special focus is placed on the representation of free surfaces. The following results are discussed: flow pattern in liquid domain, evaporative flux of free surface and evolution of free surface.

Keywords: Convective Deposition, Free Surface, Evaporation, Arbitrary Lagrangian-Euler (ALE) Method

1. Introduction

Deposition of micro- and nano-particles on a substrate is relevant to the manufacturing of conductive and antireflective functional coatings, surface-enhanced Raman scattering substrate and photolithography [1]. Several techniques are used to fabricate particle coatings, such as dip coating, sedimentation, electrostatic assembly, covalent attachment and convective deposition, among which convective deposition is probably the most convenient yet efficient way to deposit micro- and nano-particles [2].

Convective deposition is a material processing technique where an evaporating meniscus of a colloidal suspension is dragged along a solid substrate to deposit layers of micro or nanoparticles. The process is a typical multiphysics process where fluid dynamics, mass and heat transfer come into play in a small deforming domain, shown in Figure 1. Particles are transported to the receding contact line where evaporation is compensated by a liquid flux towards the contact line, which entrains particles at the same time. Particles transported towards the contact line feed the growth of a colloidal crystal. The principle of mass transport is similar to that of "coffee ring effect" [3], where coffee particles accumulate at the periphery of an evaporated coffee stain, except that the contact line is moving during the particles deposition process. Uniform coatings of particles have been deposited over multiple square centimeters on the time scale of minutes [1].

Previous research is focused on identifying the appropriate blade velocity for uniform particle deposition through experiments, and a simple geometric equation for particle flux which is proportional to evaporative flux of wetting film in colloidal crystal has been established [4]. However no theoretical and numerical work has been done to study the flow field within the fluid domain by which particles are transported to receding contact line. Besides, the geometry and volume of the liquid domain changes during the evaporation. Therefore some uncertainty exists in the experiments, for instance regarding the influence of relative humidity on the optimum crystallization velocity [2, 5]. In this work, we intend to gain insights of transport phenomena of convective deposition by investigating the flow pattern in fluid domain, evaporation at free surface and evolution of liquid domain numerically. Evaporation of liquid from the wetting colloidal crystal is the driven force in convective deposition, but only fluid without particles is simulated in this first stage of research. Simulations with particles and evaporation from wetting colloidal crystal are currently under development.

2. Typical Convective Deposition Process

In the experimental setup of convective deposition as illustrated by figure 1, a glass slide with thickness of 100 μm called the blade is placed at a distance h = 100 μm above a glass substrate, and the angle between blade and

substrate is α = 22.5°. A typical volume of 10 nL/25mm of liquid with particles is placed between blade and substrate, where 25mm stands for the width of glass slide. The blade is then moving at optimum speed usually indentified by a trail and error process, dragging the colloidal suspension, while the substrate is kept stationary. There are two versions of convective deposition set up, which are actually differentiated by the moving direction of blade. Moving blade toward the direction of acute angle, *i.e.* towards left in figure 1a, which has been proven to be more efficient than the one moving towards right [2], is modeled in this work.

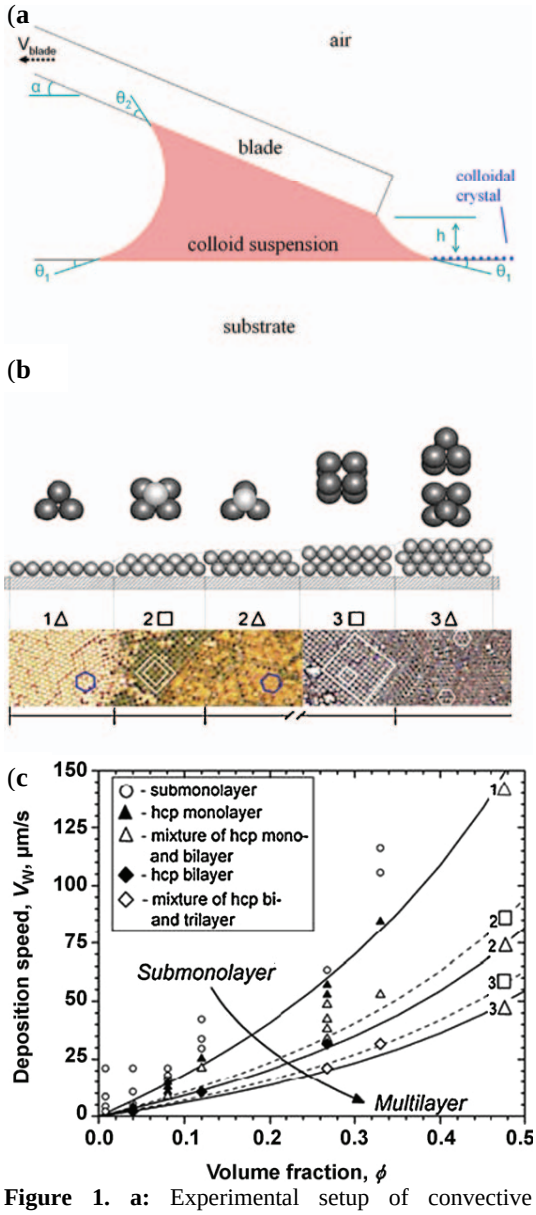

Figure 1. a: Experimental setup of convective deposition; **b**: deposited monolayer and multilayer of colloid crystal; **c**: parametric study for convective deposition [1].

The shape and radii of curvature of the two free surfaces are a function of the blade angle α, the height h between the blade and substrate, and the two wetting angles θ_1 and θ_2. θ_1 = 11°, θ_2 = 31° and R = 200 μm in this work.

The glass substrate is defined as a 4.5 × 2.1 mm rectangle. Air domain is also defined a 4.5 × 2.1 mm rectangle including liquid domain and glass slide. The effect of air domain size has not been examined, and it will be one topic for future research.

3. Multiphysics Modeling

Here we describe the governing equations, initial conditions and boundary conditions used in the modeling.

3.1 Fluid Dynamics

The liquid simulated is deionized water, and is modeled as incompressible Newtonian liquid using Navier-Stokes equations:

$$\rho\left(\frac{\partial \mathbf{v}}{\partial t}+\mathbf{v}\cdot\nabla\mathbf{v}\right)=\nabla\cdot\boldsymbol{\sigma}+\mathbf{F} \qquad (1)$$

$$\nabla\cdot\mathbf{v}=\frac{\partial u}{\partial x}+\frac{\partial v}{\partial y}=0 \qquad (2)$$

Where **v** = (u, v) is velocity vector, ρ is density of water, **σ** is stress tensor of liquid and is defined as:

$$\boldsymbol{\sigma}=\begin{pmatrix} 2\eta\frac{\partial u}{\partial x}-p & \eta(\frac{\partial u}{\partial y}+\frac{\partial v}{\partial x}) \\ \eta(\frac{\partial u}{\partial y}+\frac{\partial v}{\partial x}) & 2\eta\frac{\partial v}{\partial y}-p \end{pmatrix} \qquad (3)$$

η is dynamic viscosity of water, p is pressure, body force **F** is gravity given as **F** = (0, ρg). Air is not modeled as liquid.

Initial conditions of fluid dynamics are that the fluid is stationary: $u = 0$, $v = 0$ and $p = 2\gamma/R$, where γ is surface tension of liquid and R is radius of curvature at free surface.

Ideal boundary condition at liquid/substrate interface should be no-slip boundary condition except that contact line can move relative to substrate, which means a small portion of liquid near contact line is allowed to slip on substrate in order to comply with contact angle condition at

contact line. To model this no-slip/slip boundary condition, the liquid/substrate interface is divided into two sections by inserting points near contact line. The inserted points are 20 μm away from contact line, which ensures at least 2 mesh elements in the slip section of liquid/substrate interface.

Free surface, *i.e.* liquid/air interface, meets solid surface at an angle know as contact angle. The contact angle serves as an important boundary condition at the contact line. Two types of contact angle conditions are possible: static contact angle and dynamic contact angle [6]. Static contact angle means contact angle is constant regardless of motion of contact line, while dynamic contact angle depends on relative velocity of contact line to substrate. Dynamic contact angle condition is more accurate in physical world, but movement of contact line hardly imposes a change to contact angle in this case because the largest velocity of contact line is 100 μm/s, which is corresponding to a change of 0.1° in contact angle θ_1. A smaller velocity correlates to a even smaller change of contact angle. Thus contact angle θ_1 and θ_2 are kept constant in the simulation.

As for the liquid/blade interface, velocity of liquid is specified to be same with velocity of glass blade. This is no-slip condition at liquid/solid interface. Upper contact line of right side free surface is fixed to lower end of glass slide, therefore contact angle condition at contact line is neglected.

There are two kinds of boundary conditions at free surface: kinematic condition and stress condition. Kinematic boundary condition [7] indicates the mesh velocities at free surface and will be discussed later in ALE formulation. As for stress boundary condition, surface tension is present at the liquid/air surface:

$$\boldsymbol{\sigma} \cdot \mathbf{n} = -(2\gamma H + p_0)\mathbf{n} \qquad (4)$$

Where $\mathbf{n}$ is outward unit normal vector, H is mean surface curvature, γ is surface tension of liquid and p_0 is atmosphere pressure. In this case p_0 is set to be zero. Surface tension of liquid actually changes with temperature, which causes Marangoni convection in liquid domain due to surface tension gradient along free surface. However Marangoni effect is neglected for water because deposition of contaminants caused by high surface tension of water at free surface inhibits Marangoni convection. Surface tension is therefore kept constant for water in the modeling.

The stress condition, *i.e.* surface tension term, can be further derived to expression regarding to contact angle [7], as discussed in the numerical scheme of fluid dynamics.

3.2 Heat Transfer

Heat transfer is solved in liquid domain and substrate. Convection and radiation heat transfer for free surface exposed to air are neglected [8]. Governing equation for convective heat transfer is:

$$\rho C\left(\frac{\partial T}{\partial t} + \mathbf{v} \cdot \nabla T\right) = k\nabla^2 T + Q \qquad (5)$$

Where C is heat capacity, T is temperature, k is isotropic thermal conductivity and Q is heat source. In this case there is no heat source, thus $Q = 0$. $\mathbf{v}$ = (u, v) in liquid, while $\mathbf{v} = 0$ in solid.

Initial conditions are that liquid is at room temperature 25°C, and glass substrate is at temperature ranging from 25°C to 50°C in 5°C increment.

Temperature is kept constant as initial temperature along the side and bottom of the glass substrate. There is no heat flux at the substrate/air interface since convection and radiation heat transfer are neglected in air. Also blade/liquid interface is modeled as insulated boundary. Continuity condition is applied at Substrate/liquid interface, which means heat flux on liquid side is the same with that on substrate side. Latent heat flux from liquid to air is present at liquid/air interface due to evaporation, therefore Neumann condition for heat transfer at free surface is [8]:

$$jL = -k\nabla T \cdot \mathbf{n} \qquad (6)$$

Where j is evaporative flux and is defined in the following section of mass transport, L is latent heat of liquid evaporation.

The temperature field is coupled to fluid dynamics and mass transport. To be specific, dynamic viscosity and saturated vapor concentration at free surface are functions of liquid temperate.

3.3 Mass Transport

Evaporation process at free surface are modeled by diffusion equation for vapor

concentration in air, since convection in air is neglected:

$$D\nabla^2 c = 0 \tag{7}$$

Where c denotes vapor concentration, D is diffusivity of vapor in air. What's important is that time scale for evaporation process is three orders of magnitude larger than that for vapor concentration to adjust to changes of liquid shape and temperature, which means vapor concentration evolves in a quasi-steady manner. Therefore, time dependent term in equation (7) is zero [8].

Initial vapor concentration in the air is the product of relative humidity 0.4 and saturated vapor concentration at ambient temperature 25°C.

Similar to heat transfer, vapor concentration is kept constant as initial concentration along the side and top of air domain. Other surfaces exposed to air are modeled as insulated boundaries except for the free surface. The concentration at free surface is saturated vapor concentration which is determined by liquid temperature at free surface.

4. Numerical Implement in COMSOL

In this section, we describe the weak form of governing equations and boundary condition equations specified in section 3. Weak form equations are fundamental to the COMSOL because it is what COMSOL solves during the implement of Finite Element Method. More importantly, the scheme for moving mesh is discussed in detail.

4.1 ALE Formulation

In the convective deposition setup, colloid suspension is dragged by the moving bladed. Fixed mesh gird is therefore deemed to be inappropriate for this problem because the liquid domain is actually moving and deforming. With the help of Moving Mesh (Arbitrary Lagrangian-Eulerian, ALE) application mode in COMSOL, fluid dynamic, heat transfer and mass transport equations are solved on a deforming mesh.

The ALE method works in the following way: displacement of interior nodes are computed by propagating the moving boundary displacement throughout the domain. To obtain a smooth mesh displacement everywhere, COMSOL solves the Winslow smoothing PDE within the domain. The Winslow smoothing PDE for mesh grid coordinates (x, y) is [9]:

$$\begin{aligned} \frac{\partial^2 X}{\partial x^2} + \frac{\partial^2 X}{\partial y^2} &= 0 \\ \frac{\partial^2 Y}{\partial x^2} + \frac{\partial^2 Y}{\partial y^2} &= 0 \end{aligned} \tag{8}$$

Where (X, Y) are coordinates for mesh grid in reference frame. Reference frame is the frame in which initial mesh and initial geometry are defined before they deform. Therefore, X is initial value of x, Y is initial value of y. Equation (8) is then multiplied by test function and integrated over computational domain to obtain the weak form of equation (8). Divergence theorem is also applied to get weak form equation (9).

$$\begin{aligned} \int_\Omega \left(-\frac{\partial X}{\partial x}\frac{\partial \tilde{x}}{\partial x} - \frac{\partial X}{\partial y}\frac{\partial \tilde{x}}{\partial y}\right) d\Omega &= 0 \\ \int_\Omega \left(-\frac{\partial Y}{\partial x}\frac{\partial \tilde{y}}{\partial x} - \frac{\partial Y}{\partial y}\frac{\partial \tilde{y}}{\partial y}\right) d\Omega &= 0 \end{aligned} \tag{9}$$

Where Ω denotes computational domain, Γ denotes the boundary of computational domain. $\tilde{x}$ and $\tilde{y}$ are test functions of u and v respectively, and they are also basis function used for discretization in FEM.

Boundary mesh velocities at free surface are determined by kinematical boundary condition as mentioned before:

$$\mathbf{v}_{\text{int}} \cdot \mathbf{n} = \left(\mathbf{v} - \frac{\mathbf{j}}{\rho}\right) \cdot \mathbf{n} \tag{10}$$

Equation (10) states that normal component of boundary mesh velocity $\mathbf{v}_{\text{int}}$ at free surface equals the normal component of liquid velocity $\mathbf{v}$ at free surface minus diminishing of free surface proportional to evaporative flux $\mathbf{j}$ [8]. ρ is density of liquid. Boundary conditions for mesh deformation at horizontal boundaries are:

$$v_{mesh} = 0 \tag{11}$$

Boundary conditions for mesh deformation at vertical boundaries are:

$$u_{mesh} = 0 \tag{12}$$

Mesh movement for blade is determined by velocity of blade:

$$\begin{aligned} u_{mesh} &= u_{blade} \\ v_{mesh} &= v_{blade} = 0 \end{aligned} \tag{13}$$

One thing need to be aware of is that mesh elements become distorted in the process of deformation, and the mesh elements therefore

could have a bad quality or even become inverted. Once a mesh element becomes inverted, it is no longer eligible to solve any equation on that frame. So the whole domain should be re-meshed to avoid any inverted mesh elements at that point. COMSOL can be set to monitor quality of whole mesh elements. If the minimum quality of mesh elements drops below the criteria, the solver stops. Then a new geometry should be created from the deformed mesh at the stop point, and this new geometry could be re-meshed to get a new, well-condition mesh. Solver then is restarted based on the solution at the stop point and the new well conditioned mesh.

4.2 Fluid Dynamics

Equations of fluid dynamics are also multiplied by test function and integrated over computational domain to obtain weak form equations:

$$\int_\Omega \tilde{u}\rho(\frac{\partial u}{\partial t}+(u\frac{\partial u}{\partial x}+v\frac{\partial u}{\partial y}))-\tilde{u}\nabla\cdot\boldsymbol{\sigma}_x d\Omega=0 \quad (14)$$

$$\int_\Omega \tilde{v}\rho(\frac{\partial v}{\partial t}+(u\frac{\partial v}{\partial x}+v\frac{\partial v}{\partial y}))-\tilde{v}\nabla\cdot\boldsymbol{\sigma}_y-\tilde{v}\rho g d\Omega=0 \quad (15)$$

Where $\mathbf{e}_x$ and $\mathbf{e}_y$ is unit vector along each coordinate axis. For the continuity equation (2):

$$\int_\Omega \tilde{p}(\frac{\partial u}{\partial x}+\frac{\partial v}{\partial y})d\Omega=0 \quad (16)$$

Where $\tilde{u}$, $\tilde{v}$ and $\tilde{p}$ are test functions of *u*, *v* and *p* respectively. Apply divergence theorem to equation (14) and (15):

$$\int_\Omega \tilde{u}\rho(\frac{\partial u}{\partial t}+(u\frac{\partial u}{\partial x}+v\frac{\partial u}{\partial y}))+\boldsymbol{\sigma}_x\cdot\nabla\tilde{u}d\Omega-\int_\Gamma\tilde{u}\boldsymbol{\sigma}_x\cdot\mathbf{n}d\Gamma=0 \quad (17)$$

$$\int_\Omega \tilde{v}\rho(\frac{\partial v}{\partial t}+(u\frac{\partial v}{\partial x}+v\frac{\partial v}{\partial y}))-\tilde{v}\rho g+\boldsymbol{\sigma}_y\cdot\nabla\tilde{v}d\Omega-\int_\Gamma\tilde{v}\boldsymbol{\sigma}_y\cdot\mathbf{n}d\Gamma=0 \quad (18)$$

Since velocities at boundaries are already know, except for that at free surface, boundary integrals in equation (17) and (18) can be evaluated directly as a Dirichlet condition. Boundary intergral at free surface is evaluated separately using stress condition (4). Therefore Γ afterwards is referred as free surface. Equation (4) is reformulated as:

$$\begin{aligned}\int_\Gamma -\tilde{u}(\boldsymbol{\sigma}_x\cdot\mathbf{n})d\Gamma&=\int_\Gamma 2\tilde{u}H\gamma\mathbf{n}_x d\Gamma\\ \int_\Gamma -\tilde{v}(\boldsymbol{\sigma}_y\cdot\mathbf{n})d\Gamma&=\int_\Gamma 2\tilde{v}H\gamma\mathbf{n}_y d\Gamma\end{aligned} \quad (19)$$

By using surface divergence theorem [10], right hand side of equation (19) is derived further to two terms. One term is about contact angle at contact line that bounds free surface and another is about surface tension at free surface represented by tangential derivative variables in COMSOL. By doing this we avoid calculating mean surface curvature at free surface and we can also impose the geometrical constraint, *i.e.* contact angle condition, at contact line easily in COMSOL.

4.3 Heat Transfer

Similarly, heat transfer equations (5) are multiplied by test function and then integrated over the computational domain to obtain weak form equations:

$$\int_\Omega(\rho C\tilde{T}(\frac{\partial T}{\partial t}+v\cdot\nabla T)+k\nabla\tilde{T}\cdot\nabla T)d\Omega+\int_\Gamma k\tilde{T}\nabla T\cdot\mathbf{n}d\Gamma=0 \quad (20)$$

Boundary conditions enter equation (20) through the boundary integral terms. Dirichlet conditions at side and bottom boundaries are already known, and Neumann condition at air/substrate interface is zero, Neumann condition at air/liquid interface is given by equation (6).

4.4 Mass Transport

Mass transport equations are reformulated to weak form equations:

$$\int_\Omega -D\nabla\tilde{c}\cdot\nabla c d\Omega+\int_\Gamma D\tilde{c}\nabla c\cdot\mathbf{n}d\Gamma=0 \quad (21)$$

Boundary conditions are needed to evaluated boundary integral in equation (21). Boundary condition are specified in section 3.3.

5. Results and Discussion

5.1 Flow Pattern in Fluid Domain

For a case without evaporation, shown in figure 2, fluid is dragged by the moving blade, causing an average fluid velocity typically equal to the blade velocity. In order to better analyze

the liquid flux toward the receding contact line, the whole flow field is subtracted by the velocity of blade. Thus we obtain the relative velocity to blade. In the case without particles, a loop forms in the liquid domain with irregular shape as illustrated in figure 2. This loop is due to the two no-slip boundary conditions on the blade and substrate, which result in a shear flow, constrained by the two free surfaces.

The mesh effect on flow field can be evaluated by using different mesh in the computation. Figure 3 illustrates the velocity along the line x = 5e-4 m, which is marked in figure 2 as the vertical line at x = 5e-4 m. As seen from figure 3, velocity field converges when more than 673 mesh elements are used. For the 987 mesh elements, left free surface is divided into 40 sections while right free surface is divided into 28 sections, maximum mesh size within the liquid domain is 0.00002.

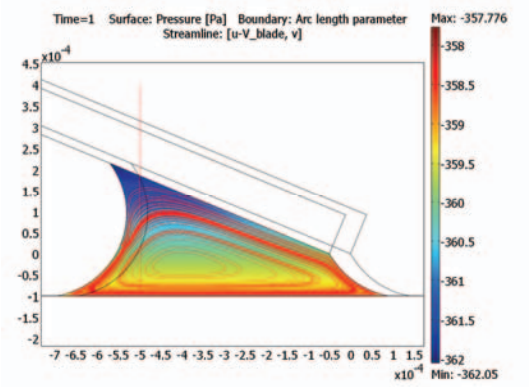

Figure 2 Flow field and pressure in the fluid domain at t = 1 s, 987 mesh elements are used. Initial shape of liquid domain is also showed as the blank frame.

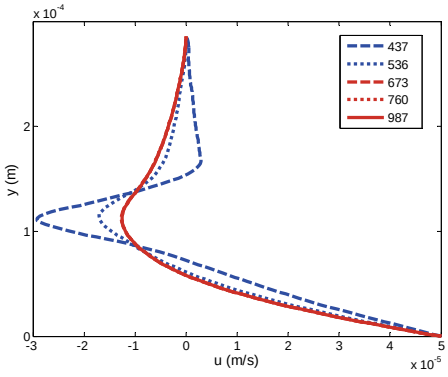

Figure 3 horizontal velocity at crossline x = -5e-4 m, t = 1s. Different mesh is used and the number of mesh elements is indicated in legend.

Different blade velocities from -30 μm/s to -100 μm/s at increment of 10 μm/s have been simulated. The position of the loop center in figure 2 relative to blade seems to be invariant for different blade velocities, which is typical given the low characteristic Reynolds number around 0.01.

5.2 Evaporative flux at right free surface

Evaporative flux at free surface is dependent on geometry of free surface, as illustrated in figure 4. Strongest evaporation is found at contact lines which indicated by left and right ends of two diffusive flux curves in figure 4. This non-uniformity in evaporative flux is due to that fact that there is more space for water vapor to diffuse to at contact line since there is no free surface on another side of contact line. While in the middle section of free surface, vapor diffusion has to face competition from nearby sections of free surface. This is also consistent with evaporation process of sessile droplet [8]. Evaporative flux at right free surface is larger than that at left free surface because the blade blocks the path of vapor diffusion towards far field of air at left side, while the right free surface is more open to environment [2].

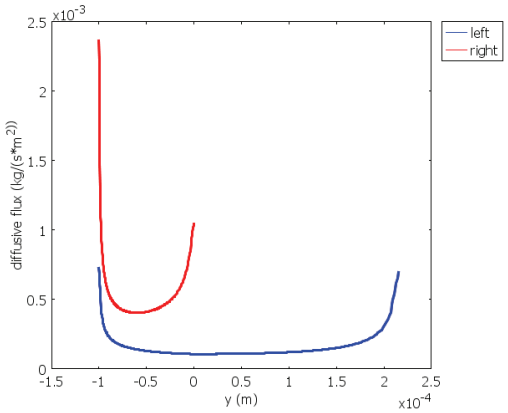

Figure 4 evaporative flux at free surface, substrate temperature 50°C, V_{blade} = 50μm/s, t = 5 s

Evaporative flux of free surface is boundary integration of evaporative flux at every point in figure 4. Diffusive flux experiences oscillations before it reaches a steady state at about t = 4 s, as illustrated by figure 5. This flux is determined by temperature of liquid at free surface when ambient relative humidity is constant, since

saturated vapor concentration is a function of free surface temperature. While the temperature of liquid is determined by substrate temperature. Saturated vapor concentration increases with temperature, therefore higher substrate temperature is corresponding to larger diffusive flux. The huge oscillations before t = 1 s in figure 5 are probably due to integration error of COMSOL.

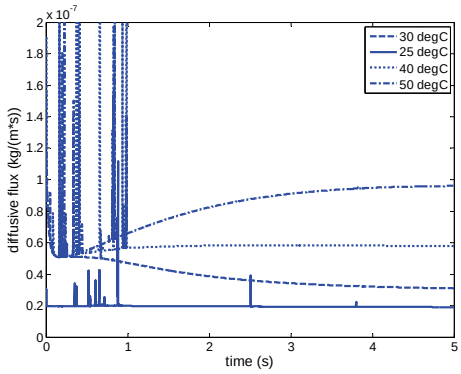

Figure 5 evaporative flux of right free surface for different substrate temperature

5.3 Radius of curvature for right free surface

Another parameter used to characterize the free surface is the radius of curvature. The radius of curvature is calculated from x-distance between upper end and lower end of free surface given that h and θ_1 are already known, assuming the free surface is a section of circle. Two cases are compared: free surface with evaporation and free surface without evaporation as presented by different lines in figure 6. Small oscillations are observed in the curves which represent the case without evaporation, a behavior that we cannot explain. However we also see that the radius of curvature decreases with time for the evaporating cases. This is explained by the fact that the radius of curvature is determined by the geometrical parameters: h, α, θ_1, θ_2 and volume of liquid. For constant h, α, θ_1 and θ_2, a smaller amount of liquid corresponds to a smaller radius of curvature.

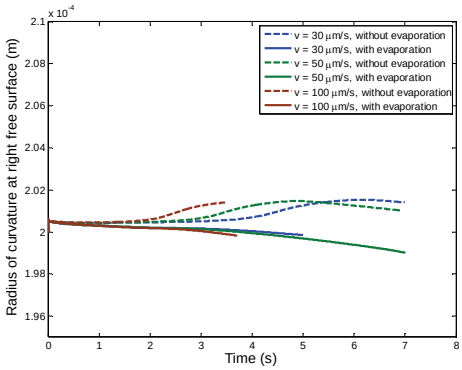

Figure 6 radius of curvature for right free surface

6. Conclusion

In this work we simulate the evaporation of a moving and deforming liquid domain used for convective deposition process by solving fluid dynamics, heat transfer and mass transfer equations using moving mesh (ALE) method. The flow relative to moving blade in the liquid domain forms a loop when no particles are simulated. While in convective deposition setup with particles, a liquid flux toward receding contact line is an important boundary condition and will be studied in the following research. We investigate the diffusive flux at free surface which is determined by geometry of free surface and substrate temperature. A higher substrate temperature is corresponding to larger evaporative flux, which means the evaporation process is speeded up. We also find that radius of curvature for free surface is decreasing with the diminishing liquid domain. This changing geometrical parameter could impose additional uncertainty to convective deposition process, thus it is another topic in the following research.

7. Acknowledgements

Junfeng Xiao gratefully acknowledges financial support for this work from the China Scholarship Council.

8. References

1. Prevo, B.G., D.M. Kuncicky, and O.D. Velev, Engineered deposition of coatings from nano- and micro-particles: A brief review of convective assembly at high volume fraction,

Colloids and Surfaces A: Physicochemical and Engineering Aspects, **311**(1-3): p. 2-10, (2007).
2. Chen, K., et al., Restricted meniscus convective self-assembly, *Journal of Colloid and Interface Science*, **344**(2): p. 315-320, (2010).
3. Deegan, R.D., et al., Capillary flow as the cause of ring stains from dried liquid drops, *Nature*, **389**(6653): p. 827-829, (1997).
4. Dimitrov, A.S. and K. Nagayama, Continuous Convective Assembling of Fine Particles into Two-Dimensional Arrays on Solid Surfaces, *Langmuir*, **12**(5): p. 1303-1311, (1996).
5. Prevo, B.G. and O.D. Velev, Controlled, Rapid Deposition of Structured Coatings from Micro- and Nanoparticle Suspensions, *Langmuir*, **20**(6): p. 2099-2107, (2004).
6. Bhardwaj, R. and D. Attinger, Non-isothermal wetting during impact of millimeter size water drop on a flat substrate: numerical investigation and comparison with high speed visualization experiments, *International Journal of Heat and Fluid Flow*, **29**(5): p. 1422, (2008).
7. Cairncross, R.A., et al., A finite element method for free surface flows of incompressible fluids in three dimensions. Part I. Boundary fitted mesh motion, *International Journal for Numerical Methods in Fluids*, **33**(3): p. 375-403, (2000).
8. Bhardwaj, R. and et al., Pattern formation during the evaporation of a colloidal nanoliter drop: a numerical and experimental study, *New Journal of Physics*, **11**(7): p. 075020, (2009).
9. *Modeling Guide of COMSOL 3.5a*.
10. Weatherburn, C.E., *Differential Geometry of Three Dimensions*. Vol. 1. 1955, London: Cambridge University Press.